Biomedical Signal Processing and Control 7 (2012) 429–437

Contents lists available at SciVerse ScienceDirect

Biomedical Signal Processing and Control

journal homepage: www.elsevier.com/locate/bspc

Automatic liver segmentation in MRI images using an iterative watershed algorithm and artificial neural network

Hassan Masoumi [a], Alireza Behrad [b], Mohammad Ali Pourmina [a], Alireza Roosta [c]

[a] Faculty of Engineering, Islamic Azad University, Science and Research Branch, Tehran, Iran
[b] Faculty of Engineering, Shahed University, Tehran, Iran
[c] Faculty of Electrical and Electronics Engineering, Shiraz University of Technology, Shiraz, Iran

ARTICLE INFO

Article history:
Received 12 June 2011
Received in revised form 14 January 2012
Accepted 18 January 2012
Available online 14 February 2012

Keywords:
MRI segmentation
Liver region extraction
Mathematical morphology
Watershed transform
Artificial neural network

ABSTRACT

Precise liver segmentation in abdominal MRI images is one of the most important steps for the computer-aided diagnosis of liver pathology. The first and essential step for diagnosis is automatic liver segmentation, and this process remains challenging. Extensive research has examined liver segmentation; however, it is challenging to distinguish which algorithm produces more precise segmentation results that are applicable to various medical imaging techniques. In this paper, we present a new automatic system for liver segmentation in abdominal MRI images. The system includes several successive steps. Preprocessing is applied to enhance the image (edge-preserved noise reduction) by using mathematical morphology. The proposed algorithm for liver region extraction is a combined algorithm that utilizes MLP neural networks and watershed algorithm. The traditional watershed transformation generally results in oversegmentation when directly applied to medical image segmentation. Therefore, we use trained neural networks to extract features of the liver region. The extracted features are used to monitor the quality of the segmentation using the watershed transform and adjust the required parameters automatically. The process of adjusting parameters is performed sequentially in several iterations. The proposed algorithm extracts liver region in one slice of the MRI images and the boundary tracking algorithm is suggested to extract the liver region in other slices, which is left as our future work. This system was applied to a series of test images to extract the liver region. Experimental results showed positive results for the proposed algorithm.

1. Introduction

Today, imaging techniques, such as magnetic resonance imaging (MRI), computed tomography (CT), and positron emission tomography (PET) are very important in the medical diagnosis process. A hepatic MR is a new diagnostic method that has experienced important advances. It produces high quality images and is one of the standard instruments for the diagnosis of liver pathologies, such as cirrhosis, liver cancer, and fulminant hepatic failure [1]. These advances include rapid scanning, new sequences of images with a high spatial resolution and more specific contrast for each type of lesion [2,3]. Fast and suitable algorithms for segmentation have an important role in the diagnosis, classification and quantitative description of diseases in various tissues, including liver tumors [4]. For example, in clinical surgery, accurate segmentation of the liver using MRI images is important for automated liver perfusion analysis, which provides important information about the blood supply to the liver [5]. Accurate liver segmentation in abdominal MRIs is challenging because the gray-level distribution of surrounding organs is not highly distinguishable. Therefore, the boundary regions between the liver and adjacent tissues generally have uniform intensity distributions, which often lead to the oversegmentation of the liver. Additionally, the vasculature inside the liver commonly leads to segmentation leakage [6].

To date, most research has been conducted on liver segmentation in CT images. Only a few studies have focused on MRI images. The primary reason that abdominal MRI research has been limited is that these images are more affected by artifacts. Moreover, they have a low gradient response, which makes accurate liver segmentation very difficult [7].

Zhang et al. [8] proposed an automatic liver segmentation method for CT images that was based on a statistical shape model (SSM) integrated with an optimal-surface-detection strategy. The method included three steps: first, the average liver shape model was determined by CT volume data via a 3D generalized Hough transform. Then, subspace initialization of the SSM was performed using intensity and gradient profiles. Finally, the shape model was reformed to adapt to the liver contour through an optimal-surface-detection approach based on graph theory.

E-mail addresses: arsam1362@yahoo.com (H. Masoumi), behrad@shahed.ac.ir (A. Behrad), pourmina@srbiau.ac.ir (M.A. Pourmina), roosta@sutech.ac.ir (A. Roosta).

1746-8094/$ – see front matter © 2012 Elsevier Ltd. All rights reserved.
doi:10.1016/j.bspc.2012.01.002

Badakhshannoory and Saeedi [9] proposed a model-based validation scheme for organ segmentation in CT scan volumes. In this method, instead of using the organ's prior information directly in the segmentation process, the information was utilized to validate a large number of potential segmentation outcomes that were generated by a generic segmentation process. For this purpose, an organ space was generated using the principal component analysis approach.

The authors of Ref. [10] proposed an automatic liver segmentation system by combining several phases of the contrast-enhanced CT images. The method employed a region-growing algorithm facilitated by pre- and postprocessing functions, which incorporated anatomical and multi-phase information to eliminate over- and undersegmentation.

Foruzan et al. [11] employed a knowledge-based technique for liver segmentation in CT images. To estimate the initial liver boundary, the method utilized a technique based on the anatomical knowledge of liver and its surrounding tissues. Furthermore, a multi-step heuristic technique was employed to segment the liver from other tissues in multi-slice CT images.

The authors of Ref. [12] proposed a liver segmentation method using a gradient vector flow (GVF) snake in CT images. This method utilized a snake algorithm with a GVF field as its external force. To improve the performance of the GVF snake in the segmentation of the liver contour, an edge map was obtained using Canny edge detector, followed by modifications using a liver template and a concavity removal algorithm.

The authors of Ref. [13] proposed a liver segmentation method from contrast-enhanced CT images. In this method, the two-step seeded region growing (SRG) method was applied on the level-set speed images to define the initial liver boundary. The first SRG efficiently divides the CT image into a set of discrete objects according to the gradient information and connectivity. The second SRG detects the objects belonging to the liver by using a 2.5-dimensional shape propagation.

Zhao et al. [14] proposed a liver segmentation algorithm in CT images, where a thresholding method was used to remove the ribs and spines in the input image. Additionally, the initial liver region was segmented using a fuzzy C-means clustering algorithm and morphological reconstruction filtering. Then, a multilayer perceptron (MLP) neural network was employed for the segmentation.

The authors of Ref. [15] proposed an automatic liver segmentation method in abdominal CT images. At first, the liver tissue is roughly distinguished by using a statistical model-based approach. Then, a force-driven optimized active contour (snake) [16,17] is applied to obtain a smoother and finer liver contour.

Different algorithms have also been proposed for liver segmentation in MRI images. Chen et al. [5] employed a multiple-initialization level set method (LSM) to overcome the leakage and oversegmentation problems in liver segmentation from MRI images. They first evolved the multiple-initialization curves separately using a fast marching method and LSMs, which were then combined with a convex hull algorithm to obtain a rough liver contour. Finally, the contour was refined again using global level set smoothing algorithm to determine the precise liver boundary.

The authors of Ref. [18] proposed a liver perfusion analysis based on active contours and chamfer matching (CM) [19,20] that were employed for liver segmentation and to align the slices in the MRI series, respectively. To apply CM, a prior liver shape image was employed to assist in the liver shape extraction and remove artifacts.

Gloger et al. [21] proposed a three-step liver segmentation method using LDA-based probability maps for multiple contrast MR images. The method is based on a modified region growing approach and a thresholding algorithm. In this method, all available MR-channel information for different weightings was used to identify liver tissue and position probabilities in a probabilistic framework. The method utilized a multiclass linear discriminant analysis to generate the probability maps for the segmentation.

Yuan et al. [6] proposed an automatic liver segmentation algorithm based on fast marching and improved fuzzy clustering methods in abdominal MRI images. This method includes four successive steps. First, the fast marching method and convex hull algorithm were applied to roughly extract the liver's boundary and topology. This step provides a basic estimation for subsequent calculations. Second, an improved fuzzy clustering method, combined with multiple-cycle processing, was designed to refine the segmentation result. Third, on the basis of the segmentation results, the liver is visualized by the marching cube (MC) method.

Middleton and Damper [22] proposed a MRI segmentation algorithm based on the combination of neural networks and active contour models. In this method, a perceptron neural network was trained to classify each image pixel as either a boundary or a non-boundary. Then, the resultant binary image was used to define the external energy function for the snake. Consequently, by minimizing the snake energy, the final result was obtained.

Most of the existing methods on liver segmentation focused on CT images. Accurate liver segmentation in abdominal MRIs is difficult because the gray-level distribution of surrounding organs is not highly distinguishable. Boundary regions between the liver and adjacent tissues generally have uniform intensity distributions, which often lead to the oversegmentation of the liver and make the automatic segmentation more difficult. Existing methods on liver segmentation in abdominal MRIs are generally semi-automatic and automatic approaches suffer from the segmentation leakage or oversegmentation.

In this paper, we propose a new method for automatic liver segmentation in abdominal MRI images. The algorithm is fully automatic and contains several stages, including preprocessing, segmentation, feature extraction and liver-region extraction. The preprocessing stage is applied to enhance the main edges of the image regions while suppressing the image noise. We then used a morphological watershed transform [4,23,24] for image segmentation because of its efficient segmentation properties. Among the various medical image segmentation methods, watershed algorithm, which is based on morphological mathematics, plays an important role. It is widely used in histology in many different ways. However, when a pure watershed transform is applied to MRI images directly, it causes oversegmentation. To overcome the problem of oversegmentation, the iterative watershed algorithm was combined with trained neural networks for image segmentation. The neural networks are trained to extract some features from the input image. The features are also extracted from the segmented image using a watershed transform. The outputs of the watershed transform are compared with the neural networks' outputs, and the difference is used to adjust the required parameters of the algorithm sequentially. To obtain optimum parameters, the parameters are gradually changed in several iterations.

The proposed algorithm deals with the extraction of the liver region in one slice of the MRI images. The slice is randomly selected from slice numbers 25–35 that have larger liver region. When the liver region is obtained for one slice, the boundary tracking algorithm may be used to extract the liver region in other slices.

The organization of the paper is as follows: Section 2 describes the proposed algorithm for liver segmentation, Section 3 represents the experimental results, and finally, we conclude the paper in Section 4.

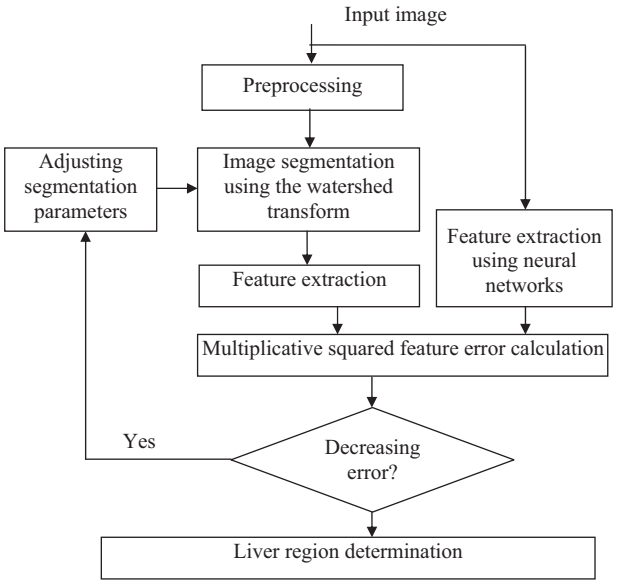

Fig. 1. Block scheme of the proposed algorithm.

2. Automatic liver segmentation system

Fig. 1 shows the block scheme of the proposed system. The proposed system is an intelligent system for liver segmentation from abdominal MRI images and consists of different stages, including preprocessing and liver extraction. The preprocessing stage consists of image enhancements, including noise reduction and edge enhancement. We apply three consecutive processes to the input image in the preprocessing stage, including morphological smoothing, Gaussian filtering and morphological gradients. The liver image extraction algorithm includes segmentation, feature extraction using an iterative watershed transform, feature extraction using the neural network and liver region determination. As shown in the figure, we used a morphological watershed transform for the liver region extraction because of its efficient segmentation properties. However, when a pure watershed transform is applied to MRI images directly, it results in oversegmentation. To overcome the problem of oversegmentation, we use a combined neural network and watershed algorithm for image segmentation as it is shown in Fig. 1. We train and use MLP neural networks to extract some features from the MRI images. The same features are also extracted after image segmentation using the watershed transform. The features that are extracted from the watershed transform are compared with the neural network outputs, and the error is used to adjust the required parameters of the algorithm sequentially. To obtain optimum parameters for the proposed algorithm, we change the parameter gradually in several iterations. The feature error, which is the multiplication of squared errors between the features extracted by the neural networks and the output of the watershed transform, is calculated in each iteration. For decreasing errors, we adjust the parameters of the algorithm and repeat the segmentation algorithm again; otherwise, the algorithm will terminate. The liver region is finally extracted using the output of the watershed transform with the optimum parameter value.

2.1. Preprocessing

Most of the abdominal MRI images are noisy, and the edges of objects are not clear in these images. Hence, the usual segmentation algorithms prevent the recognition of the main edges as well as the extraction of additional boundaries. To handle this problem, we apply preprocessing to the input image before applying the main segmentation stage. The preprocessing algorithm proposed in this paper is applied to enhance the main edges of the image regions while suppressing the image noise and insignificant regions. The preprocessing stage addresses the problem of oversegmentation by using the watershed transform.

Mathematical morphology is a suitable technique for the analysis and processing of geometrical structures based on set theory [23]. It was originally developed for binary images and later extended to gray-scale images. Mathematical morphology has been used in different areas of signal and image processing for such applications as noise filtering, image and signal enhancement and edge detection [25,26].

The proposed preprocessing algorithm is the combination of different morphological operations. Three different processes are applied to prevent the generation of insignificant regions in the main segmentation stage. These processes are morphological smoothing, Gaussian filtering and morphological gradients.

Morphological smoothing is used to suppress both bright and dark artifacts, as well as image noise. The morphological smoothing technique that is used in our system is the combination of a dilation and erosion operator, which is called a closing operator and is defined as follows:

$$\mathrm{MSI} = A \cdot B = (A \oplus B) \ominus B \tag{1}$$

where A is the input image, B is the structuring element with the desired dimensions and MSI represents Morphological Smoothed Image. In Eq. (1), $\ominus$ is defined as the erosion operator and $\oplus$ represents the dilation operator. The closing operator suppresses small dark noises in the grayscale image.

We then apply the Gaussian filter. The kernel for the Gaussian filter is calculated using Eq. (2) and applied to the output of the previous step (MSI) to produce GFI, as follows:

$$G(x, y) = \frac{1}{2\pi\sigma^2} \exp\left[\frac{(-x^2 - y^2)}{2\sigma^2}\right] \tag{2}$$

$$\mathrm{GFI} = \mathrm{MSI} * G \tag{3}$$

where σ is the standard deviation of the Gaussian filter and $*$ represents a 2D convolution. Morphological gradients are used in the third step. The image gradient makes the edge of objects more distinguishable. The subsequent usage of morphological gradients and Gaussian filters will raise the main edges and eliminate the unnecessary edges. Compared with traditional gradient operators, such as the Sobel operator, the morphological gradient produces stronger responses for ramp edges if a proper structuring element is utilized. The morphological gradient is calculated using the dilation and erosion operators, as follows [23]:

$$\mathrm{MGI} = (\mathrm{GFI} \oplus B) - (\mathrm{GFI} \ominus B) \tag{4}$$

where B is the structuring element and MGI is the gradient image. The size, shape and the direction of the structuring element are important factors to ensure proper output. We experimentally used cross-shaped structuring elements in the preprocessing stage for the smoothing and morphological gradient.

2.2. Image segmentation and feature extraction using iterative watershed transform

After applying the necessary preprocessing, the algorithm for liver region extraction is applied. Then, the watershed transform is used to extract the liver region in the abdominal MRI images. The watershed transform is a popular segmentation method utilized by the field of mathematical morphology. The watershed transform has been widely used for medical image segmentation. The method is fast and intuitive and generally does not need postprocessing

stages, such as contour joining, because it produces complete divisions of the image into separated regions, even if the contrast is poor [4].

Generally, the watershed transform is applied to the image gradient. However, applying the watershed transform directly results in myriad small regions, which is not practically useful. The preprocessing stage removes some noisy regions; however, the output is not satisfactory for automatic liver region extraction. To address this problem, we apply the watershed transform to the scaled and thresholded gradient image (STGI), where STGI is defined as follows:

$$\mathrm{STGI} = \begin{cases} \mathrm{SC} \times \mathrm{MGI} & \mathrm{MGI} > \dfrac{\min(\mathrm{MGI})}{\mathrm{SC}} \\ \min(\mathrm{MGI}) & \text{o.w.} \end{cases} \tag{5}$$

where SC is a scale factor between min(MGI)/max(MGI) and 1. The watershed transform is applied to STGI. The SC value controls the number of regions detected by the watershed transforms. For the value of SC = 1, the MGI is the same as STGI and all regions in MGI are detected by the watershed transform. Decreasing SC removes small peaks in MGI. Therefore, regions related to small peaks are removed by the watershed transform. The value of

$$\mathrm{SC} = \frac{\min(\mathrm{MGI})}{\max(\mathrm{MGI})} \tag{6}$$

removes all minimums in STGI, and no region is detected by the watershed transform. The value of SC has a major effect on the accuracy of the liver extraction algorithm. To obtain the optimum value for SC, we set SC = 1 initially and reduce the parameter gradually in several iterations to obtain the optimum SC value using the following algorithm:

- Calculate the STGI image using the current SC value.
- Segment the STGI image by applying the watershed transform.
- Select the 10 largest regions in the segmented image.
- Extract the special features for the selected regions.
- Compare the features extracted by the watershed transform with the features extracted using the neural networks, and calculate the difference.
- If the difference is decreasing, reduce the SC value and repeat the algorithm; otherwise, use the output of the watershed transform to extract liver region.

To calculate the optimum SC value, reduce the SC value linearly from SC = 1 to SC = min(MGI)/ max(MGI). We use shape-based features to obtain the optimum SC value. The liver, spleen, kidney and muscles regions are the largest regions in abdominal MRI images. Therefore, among the segmented regions by watershed transform, the 10 biggest regions are selected. Then, six shape-based features are extracted for each region: the center of the mass in the x and y directions, perimeter, area, perimeter to area ratio and minor to major axis ratio. The minor to major axis ratio for region is defined as the ratio of the minor to major axis of the ellipse that has the same normalized second central moments as the region. To make the features more robust against the size variation of the input image, we normalize the necessary features using the input image dimensions. The features are given by:

$$\mathrm{CM}x_i = \frac{\sum_{j=1}^{N_i} x_{ij}}{R \times N_i} \tag{7}$$

$$\mathrm{CM}y_i = \frac{\sum_{j=1}^{N_i} y_{ij}}{C \times N_i} \tag{8}$$

$$A_i = \frac{N_i}{R \times C} \tag{9}$$

$$P_i = \frac{M_i}{R + C} \tag{10}$$

$$R_i = \frac{M_i}{N_i} \tag{11}$$

$$\mathrm{AR}_i = \frac{\mathrm{minor\ \ axis\ \ length}_i}{\mathrm{major\ \ axis\ \ length}_i} \tag{12}$$

where $\mathrm{CM}x_i$, $\mathrm{CM}y_i$, A_i and P_i are the normalized center of mass in x and y directions, normalized area and normalized perimeter for region i, respectively. R_i is the ratio of the perimeter to the area for the region i, and AR_i is minor to major axis ratio. R and C are also the height and width of the input image, and M_i and N_i are the number of pixels in the area and the perimeter of region i, respectively.

2.3. Features estimation using neural network

To estimate the required features for the input image without segmentation, the MLP neural network configuration is used. Six different neural networks are utilized, which are trained individually for the estimation of the six previously discussed features. Neural networks are trained by the back propagation algorithm (BPA) with gradient descent minimization [27]. To obtain inputs for the neural networks, the morphological gradient of the input image is calculated. Then, the input and gradient image are normalized to the constant size of $m \times n$, and the average pixel values are calculated for the rows of normalized images. The averaged result is a vector of size m for each image, which results in feature vector size of $2m$ for the training and testing of neural networks. We used three layer neural networks with $2m$ neurons in the input layer and one neuron in output layer. The neuron for output layer shows the extracted feature, and its value during the training stage is determined by manually segmenting the liver region in the input image and calculating the related normalized feature value.

2.4. Liver region extraction

Our algorithm for liver region extraction is an iterative algorithm where the SC values decrease iteratively. With each iteration, the shape features are calculated for the 10 largest regions extracted using the watershed transform. The features are also calculated for input image using the trained neural networks as well. Then, the features that were extracted using the watershed transform are compared with the features extracted from the neural networks, and the multiplicative squared feature error (MSFE) is calculated. To calculate the MSFE, we first calculate the multiplicative squared error between the features of region i and the features calculated from the neural networks, as follows:

$$\begin{aligned} E_i = {} & (\mathrm{CM}x_i - \mathrm{CM}x)^2(\mathrm{CM}y_i - \mathrm{CM}y)^2(A_i - A)^2 \\ & \times (P_i - P)^2(R_i - R)^2(\mathrm{AR}_i - \mathrm{AR})^2 \end{aligned} \tag{13}$$

where $\mathrm{CM}x$, $\mathrm{CM}y$, A, P, R and AR are features extracted by the neural networks, $\mathrm{CM}x_i$, $\mathrm{CM}y_i$, A_i, P_i, R_i and AR_i are features of region i extracted by the watershed transform and E_i is the error for region i. The MSFE is considered the minimum of E_i, as follow:

$$\mathrm{MSFE} = \min_{i=1}^{10}(E_i) \tag{14}$$

If MSFE is decreasing, reduce the SC value and repeat the algorithm; otherwise, we use the output of watershed transform to extract the liver region. In essence, decreasing the SC value reduces the number of the extracted regions by the watershed transform. When the optimum value for SC is obtained, the region with minimum error in Eq. (14) is considered to be the liver region.

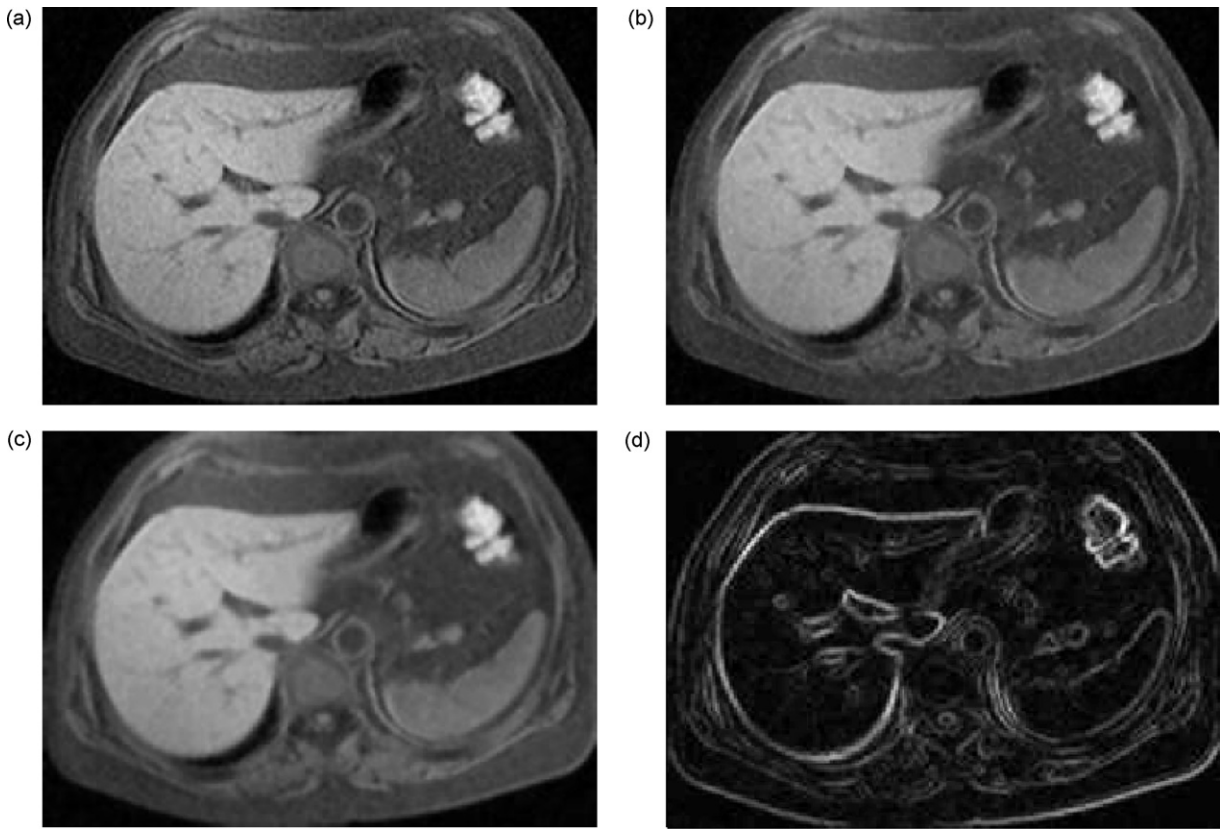

Fig. 2. The effect of preprocessing stage (a) original image, (b) the result of morphological smoothing, (c) the result of applying the Gaussian filter, (d) image after applying the morphological gradient (intensity values were scaled to enhance display quality).

3. Experiments

The proposed algorithm was implemented using a MATLAB program and tested using the collected dataset. Our dataset includes 115 abdominal MRI images with the size of 256×256 pixels that were obtained from the Imaging Center of Karaj, Iran. MRI images were obtained using a GE Medical Systems MRI machine and have the slice thickness of 5.0 mm, repetition time of 3.5 s, echo time of 1.2 s, magnetic field strength of 1.5 T, and flip angle of 55°.

We experimentally used a 5×5 Gaussian filter with $\sigma = 1$ and the cross-shaped structuring element in the preprocessing stage for the smoothing and morphological gradient, as follows:

$$B = \begin{bmatrix} 0 & 1 & 0 \\ 1 & 1 & 1 \\ 0 & 1 & 0 \end{bmatrix} \tag{15}$$

Fig. 2 shows a typical abdominal MRI image and the effect of different preprocessing stages. As it is shown in the figure, the processing stage makes the borders of different regions clearer and removes small, noisy regions.

Fig. 3 shows the effect of the *SC* value on the number of regions detected by the watershed transform for a typical MRI image. As shown in Fig. 3, the number of detected regions increases by increasing the *SC* parameter. Fig. 4 demonstrates the results of segmentation using the proposed algorithm. For comparison, the output of the watershed transform are shown for the input image, the image after preprocessing (SC = 1) and the output of segmentation with the optimum *SC* value (SC = 0.1333). Applying the watershed transform directly to the original image leads to oversegmentation, as shown in Fig. 4. When the watershed transform is directly applied to the original image, it generates 1753 regions. However, by applying the proposed algorithm and obtaining the optimal SC value, the number of detected regions decreases to 154 regions.

We used six three-layer neural networks for the extraction of shape-based features. To train the neural networks, the MRI images are normalized to the fixed size of 50×50 pixels. As mentioned before, the inputs of the neural networks are the average pixel values for the rows of normalized input and gradient images. Therefore the neural networks have 100 neurons in the first layer. We also used 10 neurons in the second layer experimentally and one neuron in the third layer. A sigmoid activation function was used in the first and second layer, and a linear function was used in the third layer.

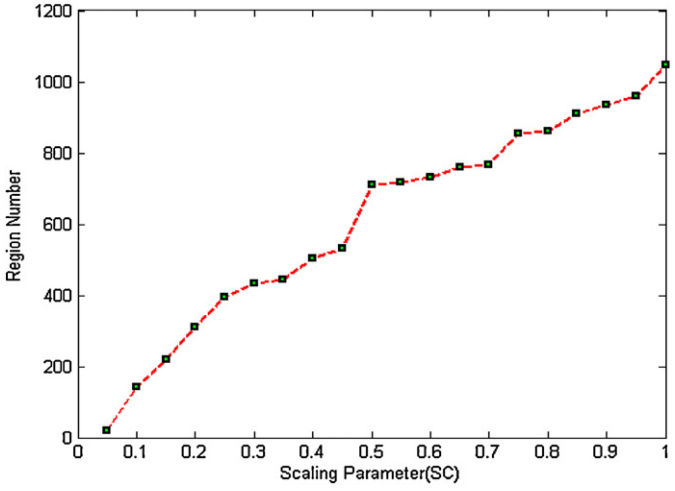

Fig. 3. The effect of the SC parameter on the number of regions detected by the watershed transform.

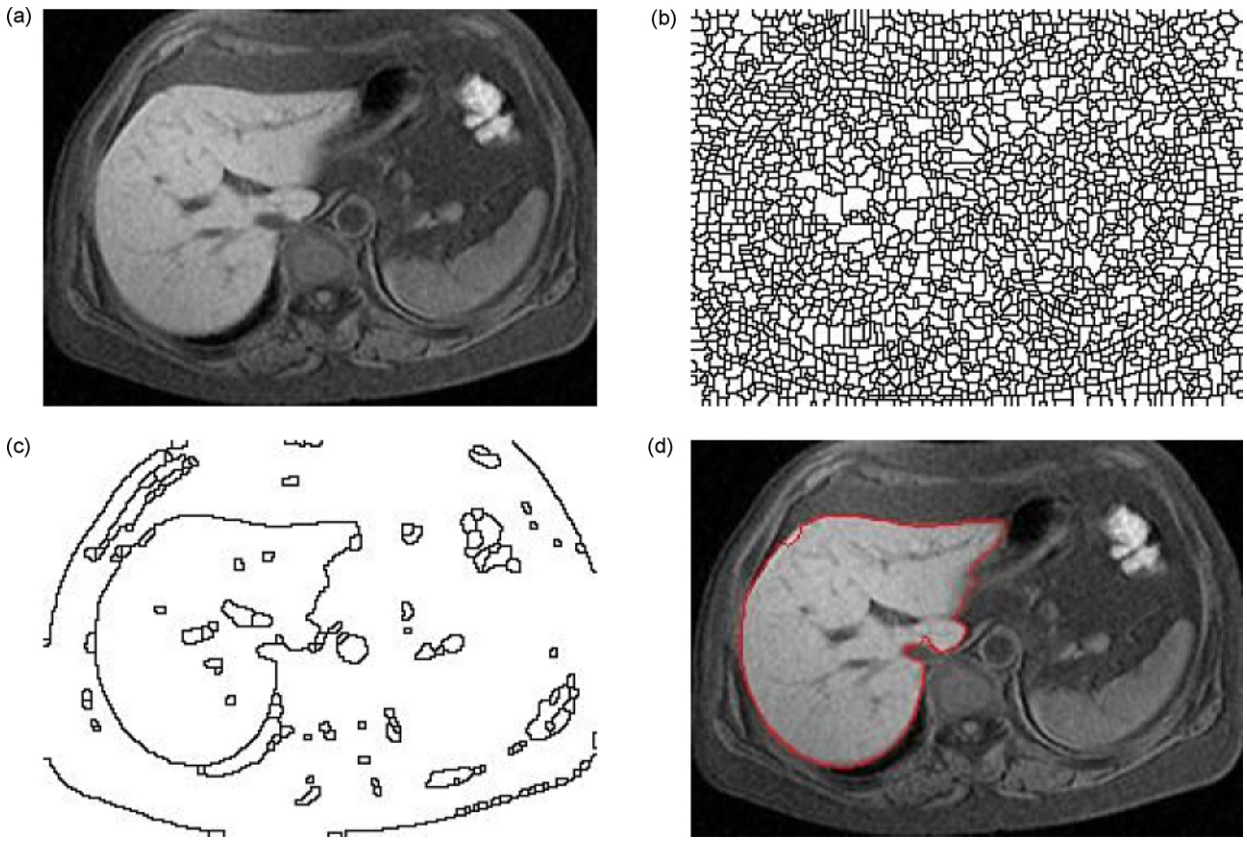

Fig. 4. Results of segmentation (a) original image (b) applying watershed transform directly to original image (c) the result of segmentation using the proposed algorithm (d) extracted liver region.

The neural networks were trained in 600,000 iterations at a learning rate of $\alpha = 0.001$. Selection of this learning rate increases the neural network training time; however, the obtained weights increase the accuracy. In this paper, 40% of the images were randomly selected for the neural network training.

Tables 1 and 2 show the values of the extracted features for 30 randomly selected test images obtained using the trained neural networks and the iterative watershed transform with the optimum SC value. Comparisons between Tables 1 and 2 show the efficiency of the training stage. The last column of Table 2 also shows the calculated MSFE. As observed in the table, the MSFEs are negligible. To compare the efficiency of the proposed algorithm with those of another method, we also implemented the method presented in Ref. [22], which is based on the active contour model. To calculate the accuracy of segmentation and compare the results of the two methods, we use the Jaccard similarity coefficient, as follows [28]:

$$\mathrm{ACC} = \frac{N(A \cap B)}{N(A \cup B)} \tag{16}$$

where the A is the liver region extracted manually by an expert, B is the liver region extracted using the algorithm, $N(A \cap B)$ is the number of pixels for the intersection of two regions A and B and $N(A \cup B)$ is the number of pixels for the union of two regions A and B. For the best case, the ACC would be 1 when the extracted region by the algorithm is the same as region extracted manually.

In Fig. 5, the accuracy of the proposed system is compared with the active contour method for 30 randomly selected MRI images. We used the same preprocessing in two methods. The average accuracy for all test images was 0.94 for the proposed algorithm and 0.92 for active contour algorithm. The active contour method is not an automatic algorithm. However, as the results show, the accuracy of the proposed algorithm is better than the active contour algorithm.

Table 1
The calculated features for 30 randomly selected images using trained neural networks.

Test images	Calculated features					
	A	CM_x	CM_y	P	R	AR
1	0.19	0.44	0.32	0.42	0.057	0.61
2	0.21	0.48	0.32	0.54	0.049	0.60
3	0.16	0.46	0.24	0.49	0.051	0.57
4	0.19	0.41	0.34	0.47	0.043	0.65
5	0.18	0.43	0.36	0.56	0.025	0.69
6	0.19	0.43	0.32	0.50	0.044	0.60
7	0.22	0.43	0.35	0.52	0.033	0.55
8	0.20	0.46	0.29	0.40	0.045	0.70
9	0.20	0.47	0.32	0.58	0.042	0.62
10	0.31	0.45	0.33	0.51	0.061	0.55
11	0.21	0.48	0.28	0.43	0.037	0.66
12	0.20	0.47	0.37	0.64	0.046	0.53
13	0.21	0.44	0.32	0.52	0.042	0.49
14	0.19	0.44	0.37	0.46	0.040	0.52
15	0.20	0.48	0.27	0.57	0.031	0.60
16	0.18	0.45	0.32	0.54	0.039	0.66
17	0.19	0.48	0.29	0.61	0.039	0.62
18	0.20	0.38	0.32	0.72	0.040	0.58
19	0.23	0.49	0.37	0.50	0.070	0.59
20	0.20	0.46	0.25	0.55	0.058	0.60
21	0.21	0.44	0.27	0.42	0.039	0.62
22	0.21	0.48	0.28	0.60	0.033	0.60
23	0.25	0.46	0.32	0.59	0.048	0.49
24	0.16	0.44	0.32	0.59	0.082	0.65
25	0.19	0.40	0.35	0.52	0.020	0.57
26	0.23	0.48	0.27	0.53	0.035	0.68
27	0.20	0.46	0.33	0.58	0.031	0.70
28	0.23	0.49	0.29	0.59	0.050	0.64
29	0.20	0.42	0.28	0.58	0.022	0.61
30	0.22	0.47	0.32	0.64	0.039	0.65

Table 2
The calculated features for 30 randomly selected images using watershed transform with optimum SC value.

Test Images	Calculated features						MSFE
	A	CM*x*	CM*y*	*P*	*R*	AR	
1	0.17	0.50	0.35	0.45	0.054	0.67	3.4348×10^{-20}
2	0.20	0.48	0.32	0.50	0.041	0.57	3.2810×10^{-26}
3	0.21	0.48	0.31	0.57	0.052	0.56	5.0797×10^{-21}
4	0.18	0.50	0.30	0.47	0.041	0.73	2.4888×10^{-21}
5	0.21	0.40	0.31	0.55	0.019	0.72	2.6475×10^{-19}
6	0.20	0.48	0.32	0.53	0.039	0.57	1.2562×10^{-22}
7	0.25	0.39	0.38	0.60	0.037	0.51	4.1598×10^{-19}
8	0.19	0.53	0.34	0.47	0.039	0.72	2.1802×10^{-19}
9	0.22	0.43	0.32	0.61	0.048	0.66	1.0421×10^{-23}
10	0.34	0.40	0.37	0.56	0.060	0.60	1.0303×10^{-19}
11	0.21	0.51	0.32	0.52	0.040	0.69	1.0605×10^{-21}
12	0.23	0.45	0.29	0.66	0.042	0.60	3.1175×10^{-20}
13	0.21	0.43	0.32	0.56	0.044	0.53	3.6283×10^{-28}
14	0.26	0.39	0.38	0.52	0.045	0.51	1.2379×10^{-20}
15	0.17	0.49	0.34	0.52	0.034	0.63	4.4622×10^{-21}
16	0.19	0.51	0.30	0.54	0.033	0.72	6.6142×10^{-21}
17	0.27	0.48	0.32	0.59	0.043	0.66	2.7128×10^{-23}
18	0.25	0.36	0.36	0.69	0.036	0.52	4.4585×10^{-20}
19	0.22	0.47	0.37	0.53	0.079	0.63	1.5163×10^{-22}
20	0.22	0.43	0.30	0.55	0.055	0.64	7.4839×10^{-24}
21	0.18	0.47	0.31	0.47	0.041	0.69	1.2368×10^{-19}
22	0.23	0.49	0.32	0.56	0.039	0.62	2.4821×10^{-21}
23	0.29	0.41	0.32	0.61	0.040	0.56	3.4742×10^{-23}
24	0.17	0.52	0.25	0.63	0.088	0.73	1.6491×10^{-18}
25	0.23	0.42	0.33	0.57	0.024	0.58	1.1597×10^{-21}
26	0.26	0.45	0.31	0.57	0.033	0.70	1.3800×10^{-21}
27	0.20	0.50	0.33	0.55	0.032	0.66	6.3593×10^{-24}
28	0.28	0.44	0.36	0.54	0.042	0.66	7.8214×10^{-19}
29	0.24	0.42	0.32	0.59	0.026	0.65	5.3213×10^{-23}
30	0.29	0.48	0.32	0.69	0.031	0.70	9.1379×10^{-21}

Although the proposed algorithm is automatic, the results of the algorithm are more satisfactory than semi-automatic approaches that require human intervention. In addition, our implementation reveals that the proposed algorithm is at least 1.5 times faster than the active contour method.

As mentioned before, to calculate the optimum SC value, we decrease the SC value linearly from SC = 1 to SC = min(MGI)/ max(MGI). The SC value is reduced in steps of ΔSC, which is determined using the following equation:

$$\Delta SC = \frac{1 - \min(MGI)/\max(MGI)}{K} \quad (17)$$

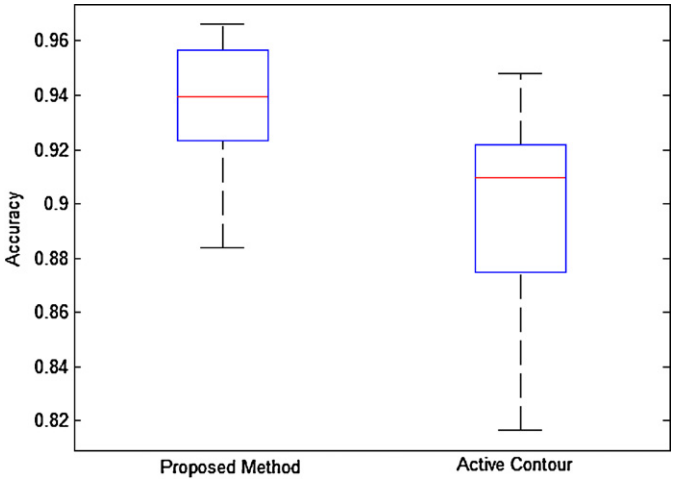

Fig. 5. Accuracy of active contour [22] and the proposed method for liver region extraction.

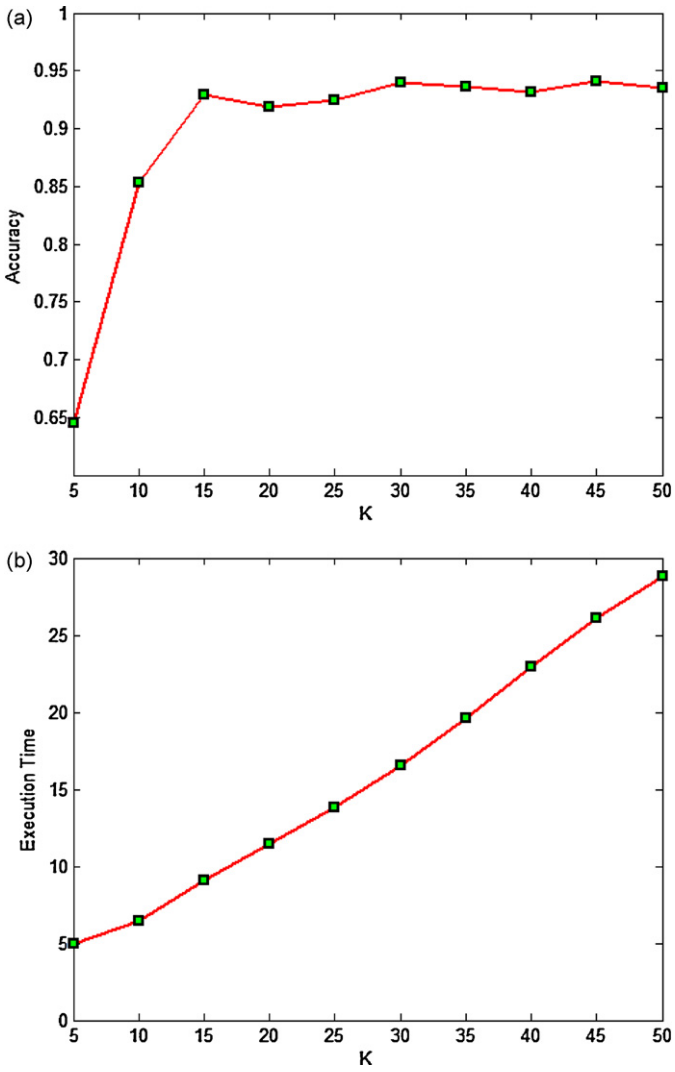

Fig. 6. The effect of the iteration number on the accuracy and execution time of the proposed algorithm, (a) average accuracy versus *K* values, (b) average execution time versus *K* values.

where *K* is the maximum iteration number for obtaining the optimum SC value. Fig. 6 shows the average execution time and the average accuracy for 10 randomly selected MRI images. As shown in the figure, increasing the *K* value increases the accuracy and the computation burden of the algorithm. However, the increase in the accuracy after *K* = 15 is negligible. Therefore, we used *K* = 15 in the experiments.

3.1. Generality of the proposed algorithm

The proposed algorithm is not only suitable for the segmentation of the liver in abdominal MRI images but also applicable to segment other regions in different medical imaging modalities with some minor changes. It is only necessary to retrain the neural networks for the new region. It is also possible to use different shape-based features. In [29], we proposed an automatic spleen segmentation algorithm using the proposed architecture. In this paper, we similarly utilized MLP neural networks with three layers. Four features were utilized in this paper for spleen segmentation, including the normalized center of mass in *x* and *y* directions, the normalized area and normalized perimeter. Because the spleen area is smaller than the liver, the 20 regions with the largest areas were selected for feature extraction using the output of the watershed

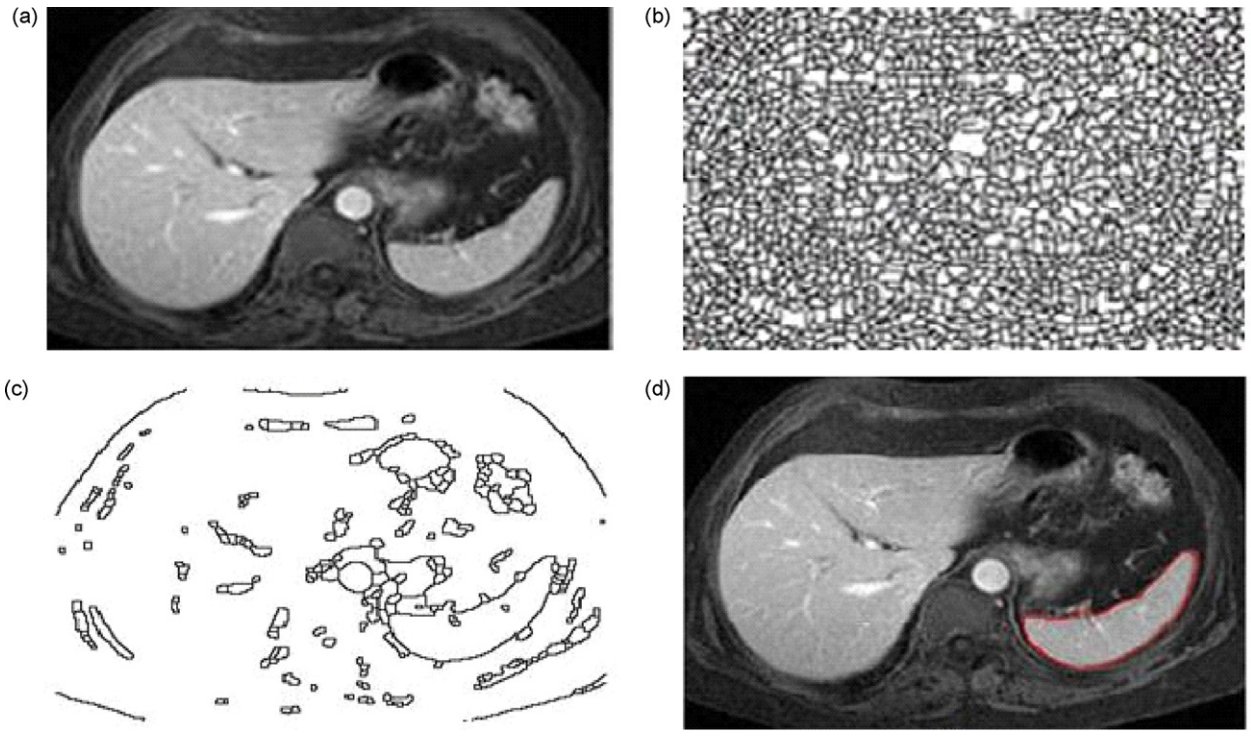

Fig. 7. Spleen segmentation using the proposed algorithm (a) original image (b) applying watershed transform directly to the original image (SC = 1) (c) applying watershed transform to the processed image with optimum SC value (optimum SC = 0.1612) (d) extracted spleen region.

Table 3
Accuracy of active contour [22] and proposed methods for spleen region extraction.

Test image	Method	
	Active contour	Proposed method
1	0.85	0.87
2	0.89	0.91
3	0.91	0.92
4	0.86	0.91
5	0.81	0.83

transform. Fig. 7 presents the results of spleen segmentation using the proposed algorithm of abdominal MRI. For comparison, the output of the watershed transform is shown for the input image and the output image with preprocessing and the optimum SC value (SC = 0.1612). Applying the watershed transform to the input image leads to oversegmentation, as shown in Fig. 7b. In this case, the watershed transform segments the input image to 2163 regions. By applying the proposed algorithm, the number of detected regions decreases to 223 regions. As shown in Fig. 7d, the spleen region is segmented completely.

Table 3 illustrates the accuracy of the spleen region extraction using the active contour method and the proposed algorithm. The results in the table demonstrate the efficiency of the algorithm for spleen region extraction.

4. Conclusions

In this paper, we introduce a new automatic system for liver segmentation in abdominal MRI images. This system uses a combination of a watershed transform and MLP neural networks, where the neural networks are used to adjust the required parameters for the segmentation. By adjusting the required parameters, we could overcome the problem of oversegmentation in the watershed transform and obtain an automatic liver segmentation algorithm, which does not require human intervention. We tested the algorithm with the collected dataset of abdominal MRI images and compared the results with that of another method, which is based on the active contour model. The average accuracy, based on Jaccard coefficients, for all test images was 0.94 for the proposed algorithm and 0.92 for the active contour algorithm. In addition, our implementation revealed that the proposed algorithm is at least 1.5 times faster than the active contour method. The proposed algorithm has the capability to segment other regions, such as the spleen region in MRI images.

The proposed algorithm deals with the extraction of the liver region in one slice of the MRI images. When the liver region is obtained for one slice, the boundary tracking algorithm may be used to extract the liver region in other slices. As future work, we plan to focus on extracting the liver region in all slices of MRI images in order to measure the liver volume in abdominal MRI images.

References

[1] P. Campadelli, E. Casiraghi, G. Lombardi, Automatic liver segmentation from abdominal CT scans, in: Proceedings of 14th International Conference on Image Analysis and Processing (ICIAP), Modena, Italy, 2007, pp. 731–736.
[2] C. Bartolozzi, C.D. Pina, D. Cioni, L. Croceti, E. Batini, R. Lencioni, Magnetic Resonance: Focal Liver Lesions Detection, Characterization, Ablation, Medical Radiology, Springer, Berlin, 2005.
[3] C. Platero, J.M. Ponacela, P. Gonzalez, M.C. Tobary, J. Sanguino, G. Asensio, E. Santos, Liver segmentation for hepatic lesions detection and characterization, in: Proceedings of 5th IEEE International Symposium on Biomedical Imaging, Paris, France, 2008, pp. 13–16.
[4] V. Grau, A.U.J. Mewes, M. Alcaniz, R. Kikinis, S.K. Warfield, Improved watershed transform for medical image segmentation using prior information, IEEE Trans. Med. Imaging 23 (4) (2004) 447–458.
[5] G. Chen, L. Gu, L. Qian, J. Xu, An improved level set for liver segmentation and perfusion analysis in MRIs, IEEE Trans. Image Process. 30 (1) (2009) 94–103.
[6] Z. Yuan, Y. Wang, J. Yang, Y. Liu, A novel automatic liver segmentation technique for MR Images, in: Proceedings of 3rd International Congress on Image and Signal Processing (CISP2010), Yantai, China, 2010, pp. 1282–1286.
[7] S. Luo, Q. Hu, X. He, J. Li, J.S. Jin, M. Park, Automatic liver parenchyma segmentation from abdominal CT images using support vector machines, in: Proceedings of International Conference on Complex Medical Engineering (ICME), Tempe, AZ, USA, 2009, pp. 1–5.

[8] X. Zhang, J. Tian, K. Deng, Y. Wu, X. Li, Automatic liver segmentation using a statistical shape model with optimal surface detection, IEEE Trans. Biomed. Eng. 57 (10) (2010) 2622–2626.
[9] H. Badakhshannoory, P. Saeedi, A model-based validation scheme for organ segmentation in CT scan volumes, IEEE Trans. Biomed. Eng. 58 (9) (2011) 2681–2693.
[10] L. Ruskó, G. Bekes, M. Fidrich, Automatic segmentation of the liver from multi- and single-phase contrast-enhanced CT images, Med. Image Anal. 13 (6) (2009) 871–882.
[11] A.H. Foruzan, R.A. Zoroofi, M. Hori, Y. Sato, A knowledge-based technique for liver segmentation in CT data, Comp. Med. Imaging Graph. 33 (8) (2009) 567–587.
[12] F. Liu, B. Zhao, P.K. Kijewski, L. Wang, L.H. Schwartz, Liver segmentation for CT images using GVF snake, Med. Phys. 32 (12) (2005) 3699–3706.
[13] J. Lee, N. Kim, H. Lee, J.B. Seo, H.J. Won, Y.M. Shin, Y.G. Shin, S.H. Kim, Efficient liver segmentation using a level-set method with optimal detection of the initial liver boundary from level-set speed images, Comput. Methods Programs Biomed. 88 (1) (2007) 26–38.
[14] Y. Zhao, Y. Zan, X. Wang, G. Li, Fuzzy C-means clustering-based multilayer perceptron neural network for liver CT images automatic segmentation, in: Proceedings of Control and Decision Conference (CCDC), Xuzhou, China, 2010, pp. 3423–3427.
[15] N.H. Abdel-massieh, M.M. Hadhoud, K.A. Moustafa, A fully automatic and efficient technique for liver segmentation from abdominal CT images, in: Proceedings of the 7th International Conference on Informatics and Systems, Cairo, Egypt, May 2010, pp. 1–8.
[16] M. Kass, A. Witkin, D. Terzopolous, Snake active contour models, Int. J. Comp. Vision 1 (4) (1987) 321–331.
[17] T. Chan, L. Vese, Active contours without edges, IEEE Trans. Image Process. 10 (2) (2001) 266–277.
[18] G. Chen, L. GU, A novel liver perfusion analysis based on active contours and chamfer matching, in: Medical Imaging and Augmented Reality, Springer-Verlag, Berlin, Germany, 2006, pp. 108–115 (Lecture Notes in Computer Science 4091).
[19] H.G. Barrow, J.M. Tenenbaum, R.C. Bolles, H.C. Wolf, Parametric correspondence and chamfer matching: Two new techniques for image matching, in: Proceedings 5th Int. Joint Conf. Artif. Intell., San Francisco, CA, USA, 1977, pp. 659–663.
[20] G. Borgefors, Hierarchical chamfer matching: a parametric edge matching algorithm, IEEE Trans. Pattern Anal. Mach. Intell. 10 (6) (1988) 849–865.
[21] O. Gloger, J. Kühn, A. Stanski, H. Völzke, R. Puls, A fully automatic three-step liver segmentation method on LDA-based probability maps for multiple contrast MR images, Magn. Reson. Imaging 28 (16) (2010) 882–897.
[22] I. Middleton, R. Damper, Segmentation of magnetic resonance images using a combination of neural networks and active contour models, Med. Eng. Phys. 26 (1) (2004) 71–86.
[23] R.C. Gonzalez, R.E. Woods, Digital Image Processing, 2nd ed., Prentice-Hall, USA, 2002.
[24] S.Y. Chien, Y.W. Huang, L.G. Chen, Predictive watershed: a fast watershed algorithm for video segmentation, IEEE Trans. Circuits Syst. Video Technol. 13 (5) (2003) 453–461.
[25] P. Maragos, Differential morphology and image processing, IEEE Trans. Image Process. 5 (1996) 922–937.
[26] J.S.J. Lee, R.M. Haralick, L.G. Shapiro, Morphological edge detection, IEEE J. Robot. Automat. 3 (1987) 142–156.
[27] M.T. Hagan, H.B. Demuth, M. Beale, Neural Network Design, PWS Publishing Company, Boston, 1996.
[28] P.N. Tan, M. Steinbach, V. Kumar, Introduction to Data Mining, Addison Wesley, Boston, 2005.
[29] A. Behrad, H. Masoumi, Automatic spleen segmentation in MRI images using a combined neural network and recursive watershed transform, in: Proceedings of 10th Symposium on Neural Network Application in Electrical Engineering, Belgrade, Serbia, 2010, pp. 63–67.